Article

Selective Extraction of Ni from Superalloy Scraps by Molten Mg-Zn

Qinghua Tian [1,2,3], Xiangdong Gan [1,2,3], Fuhui Cui [1,2,3], Dawei Yu [1,2,3,*] and Xueyi Guo [1,2,3,*]

1   School of Metallurgy & Environment, Central South University, 932 Lushan South Road, Changsha 410083, China; qinghua@csu.edu.cn (Q.T.); ganxiangdong185@csu.edu.cn (X.G.); fuhuicui@csu.edu.cn (F.C.)
2   Hunan Key Laboratory of Nonferrous Metal Resources Recycling, Changsha 410083, China
3   National & Regional Joint Engineering Research Center of Nonferrous Metal Resources Recycling, Changsha 410083, China
*   Correspondence: dawei.yu@csu.edu.cn (D.Y.); xyguo@csu.edu.cn (X.G.)

Abstract: Bearing significant concentrations of high value and critical metals, superalloy scraps require comprehensive recycling for metal reclamation. In this study, nickel-based superalloy was treated with molten Mg-Zn for the selective extraction of nickel. The influence of heating temperature, the molar ratio of Mg to Zn in the molten metal, Mg-Zn/superalloy mass ratio, and heating time on metal extraction were investigated. Using the heating temperature of 800 °C, the Mg/Zn molar ratio of 9/1, the Mg-Zn/superalloy mass ratio of 5/1, and heating time of 240 min, the extraction rate of 97.1% was achieved for Ni, and the extraction rates of Fe, Cr and refractory metals (Nb, Mo and Ti) were all less than 1%. In the subsequent vacuum distillation process, nickel with a purity of 98.3 wt% was obtained. Therefore, the proposed method is a short, clean, and efficient process for selectively extracting nickel from the superalloy scraps.

Keywords: extraction; superalloy; magnesium; zinc; nickel; vacuum distillation

1. Introduction

As a critical metal, nickel has become irreplaceable in metallurgical and some other newly-developed industries (e.g., in the manufacturing of cathode materials of the Li-ion rechargeable batteries [1]). As a limited non-renewable resource, recycling for the reclamation of Ni needs to be considered for narrowing the sustainability gap [2]. Ni-based superalloy is the core material for manufacturing hot-end parts of aerospace engines and large power equipment, which contains a large amount of nickel, cobalt, and rare elements such as molybdenum, rhenium, tungsten, and hafnium [3]. A large amount of alloy scraps is generated during the processing and use of nickel-based superalloys. Considerable amounts of the superalloy scraps are degraded, resulting in the waste of many strategic metal materials [4]. Nickel-based superalloy scraps have a high recycling value, which contains rare and precious metals such as rhenium, ruthenium, iridium, hafnium, etc., which are scarce and expensive. Therefore, there is an urgent need to develop large-scale treatment processes and recycling technologies for reclaiming valuable metals from the scrap superalloys [5,6]. Nickel is mainly extracted from laterite nickel ore (Ni, 0.8–3.0 wt%) and nickel sulfide ore (Ni, 0.3–2.0 wt%) [7,8]. Extracting nickel from natural resources requires long pyrometallurgical or hydrometallurgical routes, or a combination of both, resulting in the generation of large amounts of solid waste or wastewater [9,10]. Therefore, the recovery of nickel from secondary resources becomes ever-increasingly essential, driven by the future demand for nickel [1].

The recycling process of superalloy scraps is mainly divided into three categories: pyrometallurgy, hydrometallurgy, and pyro-hydrometallurgy. The general pyrometallurgical process encompasses secondary melting of the superalloy scraps in a vacuum induction furnace or electro-slag furnace to obtain an alloy melt, which is then processed

through separation and purification processes to remove the inclusions of non-metallic substances and obtain new alloy ingots [11–13]. Pyrometallurgy has the advantages of high efficiency and short flow, but it is easy to cause metal losses during the alloy remelting [14]. The hydrometallurgical process uses acid solution (such as HCl [15,16], H_2SO_4 [17,18], or HCl + HNO_3 [19,20]) or electrolysis [21] to dissolve the valuable metals from the scraps into the solution in the form of ions. The difference in the chemical properties of the metal elements is explored to separate and purify the metal elements through extraction, precipitation, and ion exchange processes. The hydrometallurgical process has relatively low investment, low energy consumption, and high selectivity for metal extraction. But its efficiency is comparatively low, and the generation of effluent and hazardous residues require further treatment, adding to the operational cost. Pyro-hydrometallurgy often uses pretreatment, such as alkali melts [22], oxidation [23], or low-melting metals (such as Al [24], Zn [25]) to change the characteristics of high hardness and good stability of the superalloy, followed by a series of hydrometallurgical methods to realize the extraction and recovery of alloy elements [26]).

Considering the problems associated with the traditional pyro or hydrometallurgical processes, an innovative approach was investigated for the clean and efficient processing of superalloy scraps, using molten metal to selectively extract nickel from superalloy scraps, which can potentially avoid the main problems of the traditional pyro- or hydrometallurgical processes. The underlying principle of this method is based on the solubility difference of the metals contained in scrap superalloys in the molten metal extraction medium. The selection criteria of molten metal extraction medium are: low melting point, selective dissolution of target metal, and high vapor pressure at relatively low temperatures allowing subsequent easy separation by vacuum distillation [27].

The Ni recovery process using molten metal has been studied extensively. Okabe et al. found that Ni and refractory metals in the superalloy scraps could be separated by utilizing the density differences between the Zn-Ni alloy and the refractory metals in molten Zn [28]. As shown in supplementary Figure S1 (refer to supplementary material), Zn-Ni forms intermetallic alloys; hence, it is expected that Zn exhibits a strong chemical affinity for Ni and dissolves Ni easily. Cui et al. developed a method for extracting nickel (Ni) from superalloy scraps using molten magnesium (Mg), which exhibited a strong chemical affinity for Ni and also a large solubility of Ni at high temperature (supplementary Figure S2). Subsequent vacuum treatment of the magnesium alloy allowed the distillation of Mg, forming Ni with a purity of 95.5 wt% [29]. Lee et al. investigated the recovery of nickel from Fe-Ni alloy scrap by treating it with molten magnesium, dissolving only the Ni component, and then removing Mg using the vacuum distillation [30]. In these studies, most vaporized magnesium was condensed on the inner wall of the reactor during the vacuum distillation. The condensed Mg appeared to be an aggregation of very fine Mg particles, which is prone to ignition/explosion after in contact with air. Hence, it requires a harsh operating environment to reduce the risk of explosion [31]. In the case of treating with molten Zn, the produced sponge-shaped metal residue contained Ni with a low purity of only 85.3 to 86.1 wt%, showing significant room for improvement. To overcome the hurdles mentioned above, we propose to use molten Mg-Zn as the extraction medium. As seen from supplementary Figure S3, Zn and Mg can form alloys with certain proportions. By using the binary Mg-Zn molten metal, the selectivity and high extraction rate of nickel can potentially be realized with the presence of Mg, while the addition of Zn will result in the condensation of Mg-Zn alloy after vacuum distillation, thereby reducing the risk of explosion and improving the materials while handling in a safe manner. Supplementary Figure S4 shows the vapor pressure of Mg, Zn, and the other common metal constituents (Ni, Co, Cr, Ti, Al) in nickel-based superalloy. There is an order of magnitude difference in the vapor pressure among magnesium, zinc, and other metals. Therefore, the Mg and Zn could be distilled and removed easily via heating the obtained Mg-Zn-Ni alloy.

The optimum conditions for selective extraction of Ni in superalloys were evaluated to investigate the influence of heating temperature, the molar ratio of Mg to Zn, the mass

ratio of Mg-Zn to superalloy, and heating time on metal extraction. The principle flowsheet of the liquid metal extraction-vacuum distillation (LME-VD) process is shown in Figure 1.
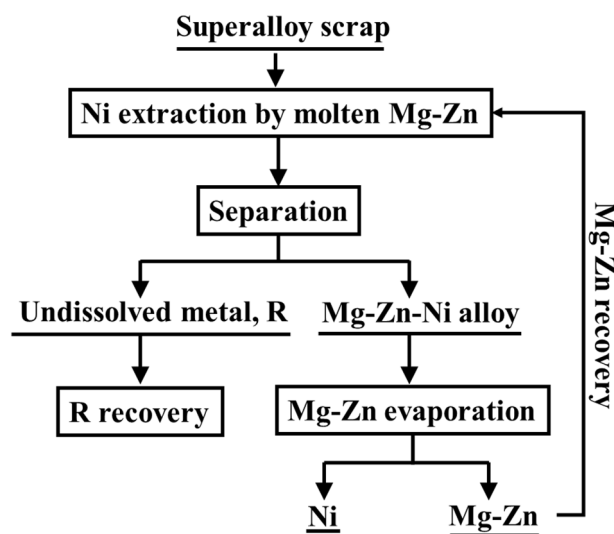

Figure 1. The principle flowsheet of the liquid metal extraction-vacuum distillation (LME-VD) process.

2. Materials and Methods

2.1. Material

The Inconel 718 superalloy was purchased from Dongbei Special Steel Group Co., Ltd, Dalian, China. Use of the newly purchased superalloy instead of scraps for the study was intended to avoid the process of cleaning the surface for the removal of oxides from scraps. More importantly, it will ensure the quality of the investigation by offering a uniform composition and a regular shape. These superalloy bars were cut by a numerical control machining into a cylindrical shape (diameter 10.6 mm, height 4–10 mm). Mg ingots (>99.9% purity) were purchased from Boyi Metal, China. Zn shots (>99.9% purity) were provided by Sinopharm Chemical Reagent Co., Ltd, Shanghai, China.

2.2. Methods

To remove the oxide layer on the surface of the magnesium ingot, the magnesium ingot was first cut into small pieces. Then the surface is polished until the silver-white metallic luster appears.

The polished Mg ingots, Zn shots, and superalloy were mixed in a graphite crucible (diameter 35 mm, height 30 mm) at a certain mass ratio. The liquid metal extraction experiment was carried out in a tube furnace (equipped with a vacuum pump) under a pure Ar (>99.999%) atmosphere. The heating rate was set as 10 °C/min from the room temperature to the target temperature during the heating-up period. An alloy ingot was obtained after cooling to room temperature. The undissolved alloy residue was situated at the bottom section of the ingot, while the top section was the Mg-Zn alloy with dissolved metals.

Vacuum distillation was performed on the top section of the obtained ingot (i.e., the Mg-Zn alloy with dissolved metals and free from undissolved alloy residue). The top section was cut off from the ingot and placed in a small graphite crucible (diameter 35 mm, height 30 mm), which was contained in a larger graphite crucible (diameter 60 mm, height 750 mm, with cover). They were placed in the tube furnace and heated at 900 °C for 360 min with a vacuum of 100 Pa to allow for distillation of Mg and Zn from the alloy, leaving dissolved metals as the residue.

Thermodynamic calculations were performed using the thermochemical software FactSage 7.1 [32]. The databases selected were FactPS, FTmisc, and FTlite.

2.3. Characterization

The chemical compositions of the superalloy, Mg ingot and Zn shot were analyzed using inductivity coupled plasma optical emission spectrometer (ICP-OES, PA6, Baird Spectrometers, Waukegan, IL, USA). The specimens (0.1–0.4 g) were completely dissolved in a mixture of HNO_3, HCl upon heating at a temperature of 150 °C for 15 min. The obtained solution was analyzed by ICP-OES. The microstructure and composition of each phase of the obtained samples were observed using scanning electron microscope with an energy dispersive X-ray spectrometer (SEM-EDS MIRA3 LMH, TESCAN, Brno, Czechia). X-ray diffractometer traces were taken on a Rigaku D/Max-2500/PC diffractometer from 10° to 100° in terms of 2θ angle using Cu Kα radiation. Table 1 lists the chemical compositions of the superalloy, Mg ingot and Zn shot. Figure 2 illustrates the XRD patterns and SEM images of the superalloy. It can be seen from Figure 2a that the matrix phases in the superalloy are mainly Cr_2Ni_3 and (Fe, Ni). Figure 2b shows the SEM image of the surface of the superalloy; it can be seen that the metal elements on the surface of the alloy are uniformly distributed.

Table 1. Chemical composition of the superalloy, Mg and Zn used in this study.

Superalloy	Element	Co	Cr	Al	Fe	Nb	Ni	Ti	Mo
	Mass percent (wt%)	0.40	19.70	0.40	17.90	4.80	52.60	0.60	3.60
Mg ingot	Element	Fe	Zn	Al	Ni	Ca	Cu	Mn	Mg
	Mass percent (wt%)	0.01	0.01	0.01	0.001	0.01	0.02	0.01	99.9
Zn shot	Element	Cu	Mg	Ni	Co	Al	Pb	Fe	Zn
	Mass percent (wt%)	0.01	0.01	0.001	0.01	0.01	0.01	0.01	99.9

Note: Analyzed by ICP-OES. Concentration of Ni is calculated as follows: C_{Ni}(mass pct) $= 100 - C_{Co} - C_{Cr} - C_{Al} - C_{Fe} - C_{Nb} - C_{Ti} - C_{Mo}$; Concentration of Mg is calculated as follows: C_{Zn}(mass pct) $= 100 - C_{Fe} - C_{Zn} - C_{Al} - C_{Ni} - C_{Ca} - C_{Cu} - C_{Mn} - C_{Mg}$; Concentration of Zn is calculated as follows: C_{Mg}(mass pct) $= 100 - C_{Cu} - C_{Mg} - C_{Ni} - C_{Co} - C_{Al} - C_{Pb} - C_{Fe} - C_{Zn}$.
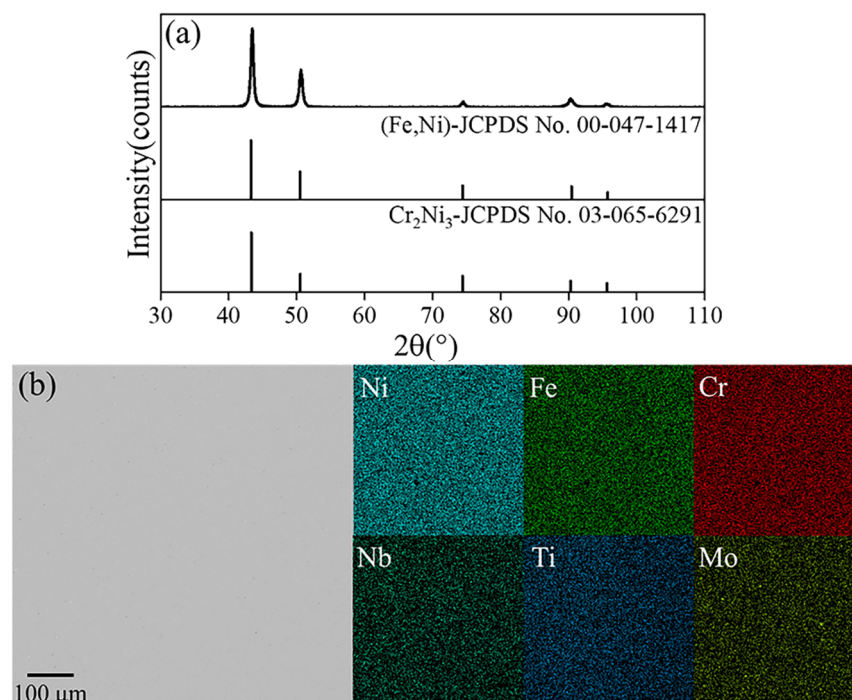

Figure 2. XRD patterns, SEM images and EDS mappings of the Ni-based superalloy: (**a**) XRD patterns; (**b**) SEM image and EDS mappings.

Dissolution degrees of various metals into molten Mg-Zn were determined by sampling the obtained alloy ingot followed by chemical analysis. Sampling was performed by sawing the Mg-Zn alloy region of the ingot using a hacksaw, generating enough splinters, which were completely dissolved into an aqueous solution before analysis using ICP-OES to determine metal concentrations in the Mg-Zn. In the experiment, the volatilization of Mg and Zn was so small that it could be ignored. The extraction of metals could be calculated by Equation (1), based on the law of conservation of mass. In this equation, the term $(m_2 - m_1 - m_3 - m_4)$ represents the total weight of Mg and Zn in the Mg-Zn alloy ingot. Therefore, the term $(m_2 - m_1 - m_3 - m_4)/(w_{Mg} + w_{Zn})$ represents the total weight of the Mg-Zn alloy ingot (containing the dissolved metals). During the experiment, the concentration of Mg and Zn in the area of alloy residue was measured by EDS and found to be very low (<10 wt%). Considering the large mass of Mg-Zn used, the weight of Mg (m_3) and Zn (m_4) in the alloy residue can be neglected in the procedure of calculation. Thus, the metal extraction could be estimated through Equation (2).

$$\eta_M = \frac{100 w_M \left[(m_2 - m_1 - m_3 - m_4)/(w_{Mg} + w_{Zn}) \right]}{m_1 w_0} \times 100\% \tag{1}$$

$$\eta_M \approx \frac{100 w_M (m_2 - m_1)/(w_{Mg} + w_{Zn})}{m_1 w_0} \times 100\% \tag{2}$$

where η_M is the extraction rate of metal M; m_1 is the weight of superalloy used in the experiment; m_2 is the total weight of the cooled sample (mixture of Mg-Zn alloy and residual alloy); m_3 and m_4 are the weight of Mg and Zn in the alloy residue, respectively; w_0 is the initial mass percentage of the metal M in the pristine superalloy; w_M is the mass percentage of the metal M in the cooled Mg-Zn alloy; w_{Mg} and w_{Zn} are the mass percentage of Mg and Zn in Mg-Zn alloy after cooling.

3. Results

The LME-VD process includes two parts: liquid metal extraction process (LME) and vacuum distillation process (VD). In the following sections, the effects of heating temperature, the molar ratio of Mg to Zn, the mass ratio of Mg-Zn to superalloy, and heating time on the extraction process were evaluated to determine the optimal extraction conditions for the selective extraction of Ni from the superalloy.

3.1. Liquid Metal Extraction Process

3.1.1. Effect of Heating Temperature

The effect of heating temperature was studied by fixing the heating time at 6 h, the mass ratio of Mg-Zn/superalloy at 5/1, and the molar ratio of Mg/Zn at 7/3; the results are shown in Figure 3. Supplementary Figure S5 is the XRD patterns of the Mg-Zn alloy under different heating temperatures.
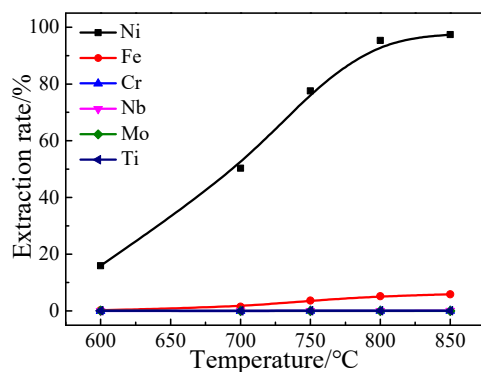

Figure 3. Effect of temperature on the extraction of metals (Note: the curves for Cr, Nb, Mo and Ti are overlapping).

As seen from Figure 3, the extraction rate of Ni firstly increased with the increasing heating temperature and reached a plateau at temperatures higher than 800 °C, in which the maximum extraction rate of Ni exceeded 95%. As seen in supplementary Figure S5, the main phases in the Mg-Zn alloy are Mg, Mg_7Zn_3, and MgZnNi. The extraction rate of Fe increased only slightly with the increasing heating temperature and reached a maximum of 5.9% at 850 °C. The maximum solubility of Fe in Mg is lower than 0.5% [33], but the extraction rate of Fe is higher than 5% at 800 °C, which can be attributed to the dissolution of Fe in Zn [34]. Comparatively, the extraction of Cr, Nb, Mo, and Ti was all lower than 2%.

In order to further prove the effect of heating temperature on the dissolution of metals into molten Mg-Zn, the equilibrium composition of metals at different temperatures was calculated using the thermochemical software Factsage. The results are given in Figure 4. As seen, the calculated extraction rate of Ni increases with the increasing temperature and reaches a plateau at approximately 340 °C. Due to the high solubility of Ni in molten Mg-Zn, further increasing the temperature has little effect on the extraction rate. The extraction rate of Fe increases gradually with the increasing temperature. The experimental data matchs relatively well with the calculated Ni and Fe results at different temperatures, with the discrepancy resulting from kinetics [35]. However, there is a considerable difference between the experimental data and the calculated results for the dissolution of Cr, Mo, and Nb, especially at higher temperatures, indicating that kinetic factors played a more significant role in their dissolution.
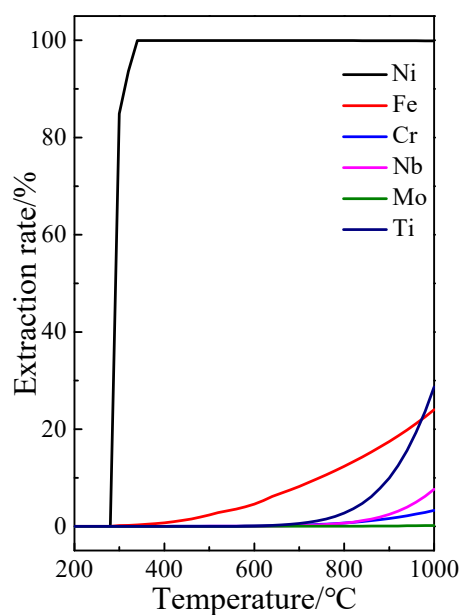

Figure 4. Simulation of the extraction process at different temperatures using Factsage [32]. (In the calculation process, it was assumed that the masses of the initial superalloy and Mg-Zn alloy were 100 g and 500 g, respectively. The Mg-Zn alloy contains 267.8 g of Zn and 232.2 g of Mg; liquid 1# in the Factsage calculation results were adopted.).

In order to demonstrate the influence of temperature on the evolution of microstructure during the extraction process, BSE images and elemental mapping of samples at 600 °C and 800 °C are presented in Figures 5 and 6, respectively.
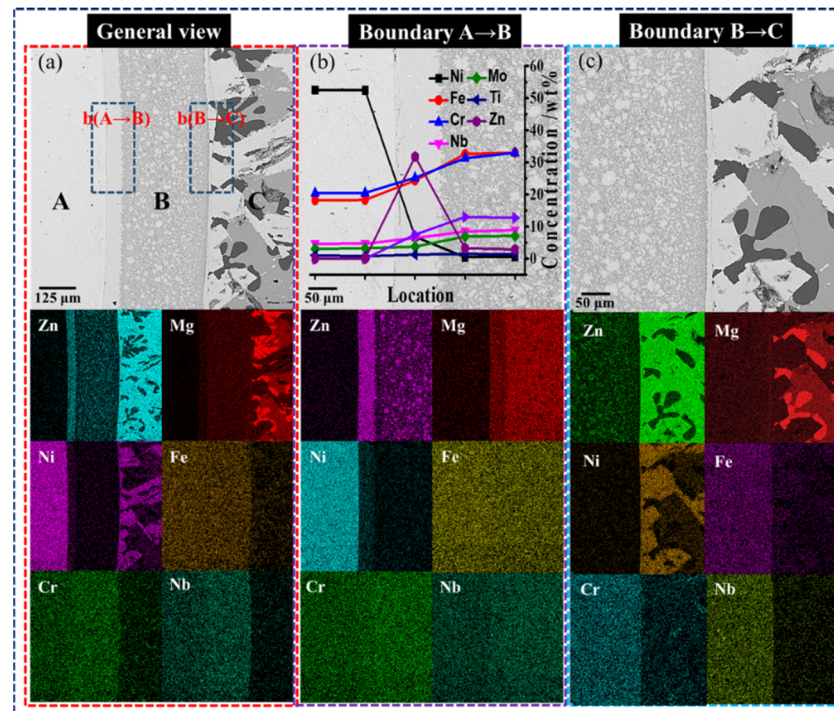
Figure 5. BSE images and elemental mapping of the sample produced from 600 °C. (**a**) SEM images of alloy and Mg-Zn alloy with a boundary; (**b**) SEM image of the alloy and residual with a boundary; (**c**) SEM images of residual and Mg-Zn alloy with a boundary; A-Unreacted superalloy; B-Residual layer rich in Fe and Cr; C-Generated Mg-Zn-Ni alloy.
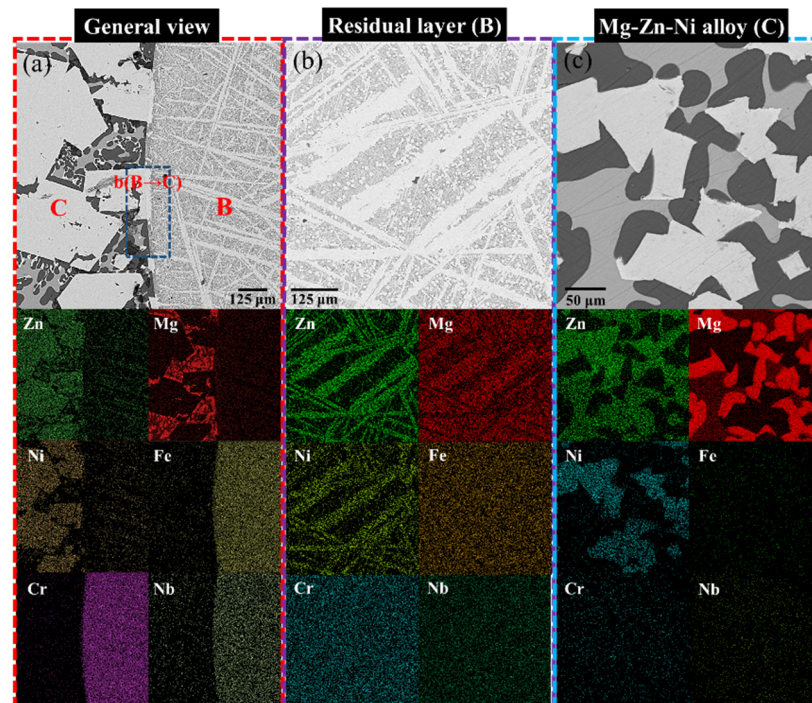

Figure 6. BSE images and elemental mapping of the sample at 800 °C. (**a**) SEM images of residual and Mg-Zn alloy with a boundary; (**b**) SEM image of the residual layer; (**c**) SEM images of Mg-Zn alloy; B-Residual layer rich in Fe and Cr; C-Generated Mg-Zn-Ni alloy.

As shown in Figure 5a, there is an obvious boundary between the alloy (A) and the Mg-Zn alloy (C), obtained after heating at 600 °C for 6 h. This would be especially of benefit

for the industrial application of the proposed process since it indicates the possibility of clean separation between the residue and the melt. The SEM images of the sample show the presence of a residual layer (B) between the virgin alloy and the Mg-Zn alloy (Figure 5a), and snowflake-shaped phases in the residual layer (Figure 5b), and polygon-shaped phase in the Mg-Zn alloy side (Figure 5c). Elemental mapping of each section indicates that the residual layer (B) mainly contained Cr, Fe, Nb, Mg, Zn, with barely any Ni (Figure 5a), and the snowflake-shaped phases are rich in Zn, Cr, and Fe (Figure 5b). The Mg-Zn alloy region mainly contained Mg, Zn, and Ni (Figure 5c). The white irregular polygon-shaped phase found in the Mg-Zn alloy region is MgZnNi, the gray phase is Mg_7Zn_3, and the dark phase is Mg (Figure 5c). At a heating temperature of 600 °C, no solid phase was formed in the alloy melt, and the MgZnNi phase gradually formed in the cooling process [36]. Interestingly, there is an intermediate layer (β) between the unreacted alloy and the residual layer. The EDS results show that the intermediate layer (β) is mainly rich in Zn (Figure 5b). It is suspected that Mg-Zn has to pass through the residual layer (B) to allow extraction of Ni from the virgin superalloy (Figure 5b). The formed residual layer is the resulting residue of superalloy after losing the base-metal Ni.

Similar to 600 °C, the SEM images of the sample produced at 800 °C has a distinguishable boundary between the residual layer and the Mg-Zn alloy (Figure 6a). The Mg-Zn alloy region has the white irregular polygon-shaped phase of MgZnNi (Figure 6c). The residual layer (Figure 6b) contains Cr, Fe, Ni, Nb, Zn, and Mg, suggesting that Mg and Zn have diffused into the residual layer. As far as the residual layer is concerned, the difference between the samples taken at 600 °C and 800 °C is that the snowflake-shaped phase disappeared at 800 °C and instead, formed the needle-shaped light phase (Figure 6a,b). Furthermore, a small amount of Cr and Nb have also diffused into the Mg-Zn alloy (Figure 6c). Additionally, samples at a higher temperature formed a wider residual layer (other conditions being the same, Figure 7), which further demonstrates that the extraction rate of Ni increases with the increasing temperature.
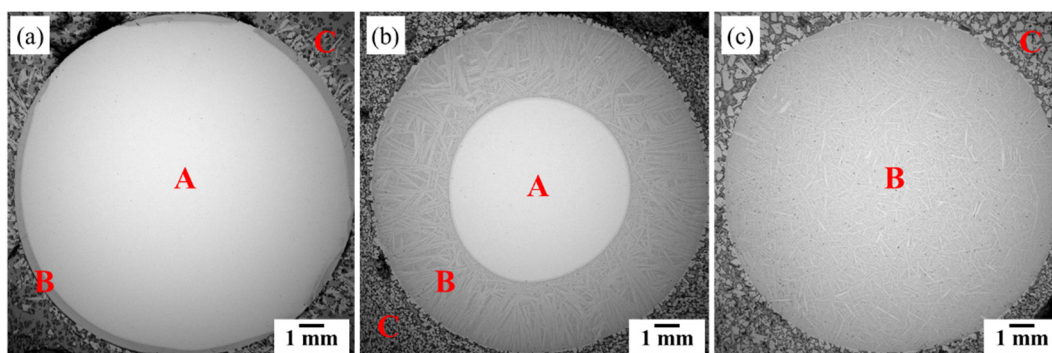

Figure 7. BSE images of the samples obtained from different temperatures: (**a**) 600 °C; (**b**) 750 °C; (**c**) 800 °C. A-Unreacted superalloy; B-Residual layer rich in Fe and Cr; C-Generated Mg-Zn-Ni alloy.

Based on the above analysis, it becomes apparent that the extraction of Ni is achieved via outward diffusion of Ni from superalloy to the molten Mg-Zn. At high temperatures, Ni on the surface of the virgin superalloy started dissolving into the surrounding molten Mg-Zn. The loss of Ni in the superalloy and the dissolubility of other elements (especially the large amount of Fe and Cr) in molten Mg-Zn resulted in the gradual formation of the residual layer. With the increase of temperature, both the diffusion rate of Ni and the maximum solubility of Ni in the molten Mg-Zn increase, resulting in a higher extraction rate at higher temperatures. In addition, the volatilization of molten Mg and Zn is promoted at higher temperatures. Therefore, the heating temperature of 800 °C was selected as the optimal temperature in the following experiments.

3.1.2. Effect of Molar Ratio of Mg to Zn

The effect of the molar ratio of Mg to Zn was investigated by fixing the heating temperature at 800 °C, the heating time at 360 min, and the mass ratio of Mg-Zn to superalloy at 5/1; the results are shown in Figure 8.
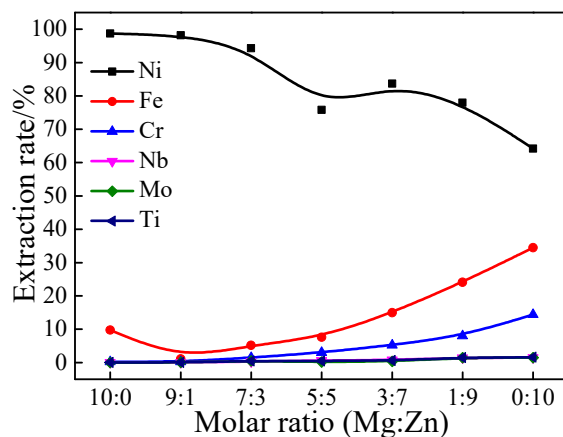

Figure 8. Effect of the molar ratio of Mg to Zn on the extraction of metals from the superalloy (Note: the curves for Nb, Mo and Ti are overlapping).

As seen in Figure 8, the extraction rate of Ni decreases with the increase of the molar percentage of Zn. A high molar percentage of Mg is beneficial for the extraction of Ni. When the molar percentage of Mg was 100%, the extraction rate of Ni was the highest (98.67%). While nearly 98.2% of Ni in the scrap could be extracted at a Mg to Zn molar ratio of 9/1, and the extraction rate reduced to 64.2% at the Mg to Zn molar ratio of 0/10. Dissolution of Fe should be minimized for the better selectivity of Ni. As seen, the extraction of Fe reached a minimum at a Mg/Zn molar ratio of 9/1, while the maximum was 34.48 wt% when the molar percentage of Zn was 100%. The maximum solubility of Fe in Mg is lower than 0.5 at% based on the Mg-Fe phase diagram, but the extraction rate of Fe is higher than 10% at a Mg/Zn molar ratio of 10/0, which is likely caused by the dissolution of Fe in the formed Mg_2Ni phase (maximum of about 14 at%) [37]. With the presence of 10 mol% Zn, the extraction rate of Fe became lower (Figure 8), which can be attributed to the suppression of the Mg_2Ni phase formation [38,39]. It is very interesting to observe (Figure 8) that the solubility decrease with increasing Zn content of the Mg-Zn melt is not monotonous. Deviations from linear behavior are ratios 5/5 (local minimum) and 3/7 (local maximum), following the two binary Mg-Zn phases. This shows that the formation of the binary Mg-Zn phase will have a certain influence on the melt extraction process [32]. When the extraction medium contained >10 mol% Zn, the extraction rate of Fe further increased with the increasing percentage of Zn, which can be attributed to the dissolution of Fe in Zn [34]. Similarly, the extraction rate of Cr also increased with the increasing molar percentage of Zn. However, the extraction of Nb, Mo, and Ti are all lower than 4%.

To further reveal the influence of the molar ratio of Mg to Zn on the dissolution of metals in molten Mg-Zn, thermochemical software Factsage was used to calculate the equilibrium composition of the simulated extraction process, the results of which are given in Figure 9. It can be seen that the calculated extraction rate of Ni remained at 100% with the increase of Zn in Mg-Zn. The reason for the mismatch with the experimental results is likely due to the limited heating time during the experiments. The extraction rate of Fe increases with the increased amount of Zn in Mg-Zn, which is in good agreement with the experimental results. However, the calculated dissolution rates of Cr, Mo, and Nb exhibit huge differences between the experimental data and calculated results at equilibrium, demonstrating the significant role of kinetics that governed the dissolution behavior [35]. Based on the above discussion, the Mg/Zn molar ratio of 9/1 was chosen as the optimum

because the highest selective extraction of Ni can be achieved at this ratio. It was therefore employed in the following experiments.
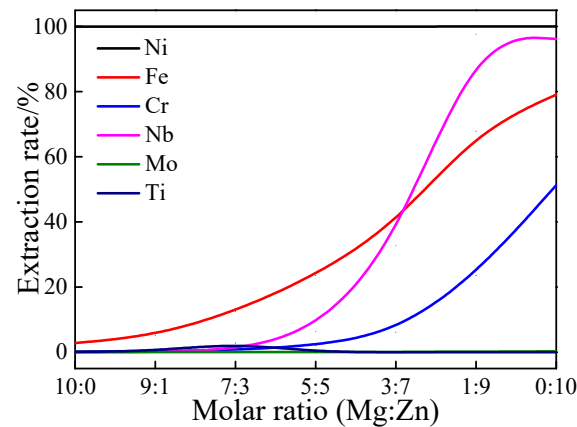

Figure 9. FactSage simulation on the extraction of metals from superalloy using a different molar ratio of Mg to Zn at 800 °C [32]. (In the calculation process, it was assumed that the masses of the initial superalloy and Mg-Zn alloy were 100 g and 500 g, respectively; liquid 1# in the Factsage calculation results was adopted.).

3.1.3. Effect of the Mass Ratio of Mg-Zn to Superalloy

The effect of the mass ratio of Mg-Zn to superalloy was studied by fixing the heating temperature at 800 °C, the heating time at 360 min, and the molar ratio of Mg to Zn at 9/1; the results are shown in Figure 10. Supplementary Figure S6 is the XRD patterns of the Mg-Zn alloy under different mass ratios of Mg-Zn/alloy.
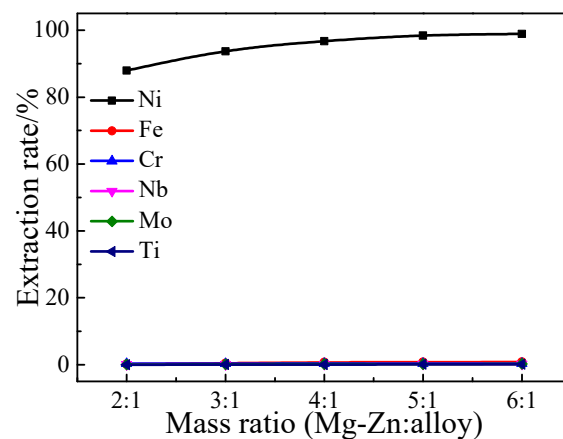

Figure 10. Effect of the mass ratio of Mg-Zn to superalloy on the extraction of metals (Note: the curves for Fe, Cr, Nb, Mo and Ti are overlapping).

As seen from Figure 10, the extraction rate of Ni increases with the increase of the mass ratio of Mg-Zn to superalloy, while the extraction rate of Fe, Cr, Nb, Mo, and Ti are steadily low throughout the range investigated. Supplementary Figure S6 shows the XRD patterns for the Mg-Zn alloy of the samples under the different mass ratios of Mg-Zn to superalloy. It can be seen that when the mass ratio is 5/1 and 6/1, the main phases of Mg-Zn alloy are Mg and MgZnNi. In the extraction process, the higher mass ratio provides an adequate Mg-Zn environment, resulting in a larger concentration gradient of Ni between the alloy residual layer and molten Mg-Zn, which enhances the continuous solution.

In order to reflect the influence of the amount of Mg-Zn on the dissolution of metals from the initial superalloy to the molten Mg-Zn, the equilibrium composition of different amounts of Mg-Zn at 800 °C was calculated by Factsage, and the results are shown in

Figure 11. As seen, the dissolution rate of Ni initially shows a nearly linear and sharp increase with the increasing dosage of Mg-Zn, with the mass ratio ranging from 0.4/1 to 2/1. Further increase in the mass ratio resulted in little change in the dissolution of Ni, resulting from the high solubility of Ni in molten Mg-Zn. The dissolution rate of Fe presents a linear and very slow increase with an increased dosage of Mg-Zn. The calculated results of the dissolution of Ni and Fe in molten Mg-Zn exhibit relatively good matching with the experimental data. It should be pointed out that the calculated results of Cr, Nb, and Mo also have significant differences compared to the experimental data, likely due to kinetic reasons. A Mg-Zn/alloy mass ratio of 5/1 was employed in the following experiments.
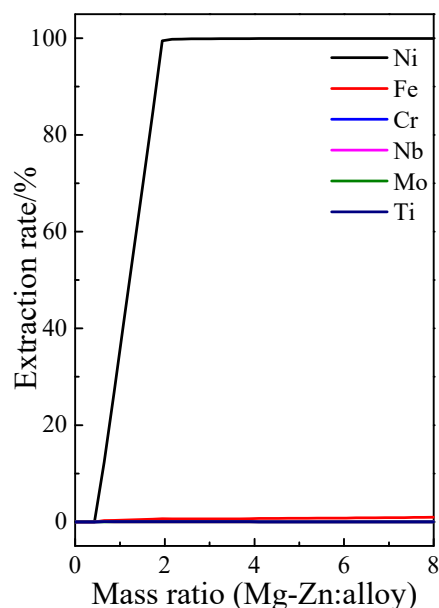

Figure 11. FactSage simulation on the extraction of metals from superalloy using different mass ratios of Mg-Zn to alloy at 800 °C and the molar ratio of Mg/Zn was 9/1 [32]. (In the calculation process, it was assumed that the mass of the initial superalloy was 100 g; liquid 1# in the Factsage calculation results was adopted. Note: the curves for Cr, Nb, Mo and Ti are overlapping).

3.1.4. Effect of Heating Time

The effect of the heating time was studied by fixing the heating temperature at 800 °C, the mass ratio of Mg-Zn/alloy at 5/1, and the molar ratio of Mg to Zn at 9/1; the results are shown in Figure 12. Supplementary Figure S7 is the XRD patterns of the Mg-Zn alloy under different time.
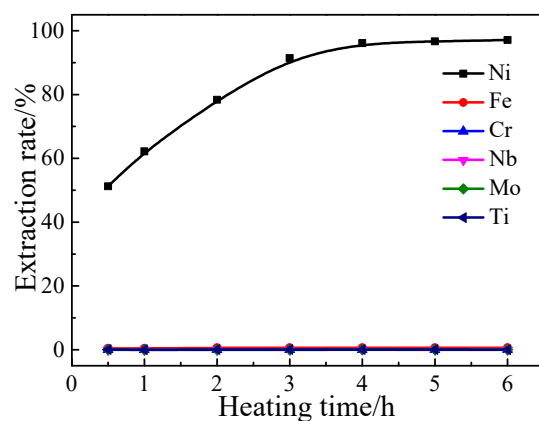

Figure 12. Effect of heating time on the extraction of metals (Note: the curves for Fe, Cr, Nb, Mo and Ti are overlapping).

As illustrated in Figure 12, the extraction rate of Ni increases steadily from 51.2% at 30 min to 96.1% at 240 min, and reaches plateau afterward. Considering the heating rate of the furnace (i.e., 10 °C/min), it required 80 min to reach the target temperature. The melting of Mg-Zn alloy (Mg/Zn molar ratio 9/1) started when the heating temperature exceeded the melting point of 412 °C (supplementary Figure S3), indicating that the linear-heating stage contributed 38.8 min to the melting of Mg-Zn alloy (Mg/Zn molar ratio 9/1). During this period, the dissolution process should have already started. As seen from Figures 5–7, dissolution of the superalloy ingot involved the formation and continuous growth of a residual layer. The outward migration of Ni started from the interface between the shrinking unreacted core and the residual layer, and its continuous outward diffusion through the entire thickness of the residual layer took place before dissolution into the molten Mg-Zn alloy surrounding the ingot. In addition, the evolution of various phases in the residual layer (Figures 5 and 6) added to the complexity of the diffusion process and the resulting selective dissolution of Ni. The high selectivity for Ni dissolution can be seen from the little dissolution of other metals (i.e., Fe, Cr, Nb, Mo, and Ti), some of which were even not detected in the Mg-Zn alloy. As shown in supplementary Figure S7, the main phases in the Mg-Zn alloy under different heating times are Mg and MgZnNi. Hence, the optimal experimental conditions were as follows: heating temperature 800 °C, Mg/Zn molar ratio 9/1, heating time 240 min, and the Mg-Zn/alloy mass ratio 5/1.

3.2. Separation of Mg-Zn Alloy by Vacuum Distillation

An ingot was firstly produced from the liquid metal extraction using the above-mentioned optimal experimental conditions. The upper part of the ingot (0 to 10 mm from the top of the sample), which was free from any residual alloy, was cut off and used for subsequent vacuum distillation. In order to allow further analysis of the alloy residue situated at the bottom of the alloy ingot, it was separated from the surrounding Mn-Zn alloy and was also subjected to vacuum distillation. Table 2 lists the ICP results for Mg-Zn alloy before distillation, the produced Ni as well as the alloy residue from distillation. As shown, the upper part of the obtained ingot contained 69.5 wt% Mg, 21.5 wt% Zn, 8.92 wt% Ni and 0.02 wt% Fe. Refractory metals such as Mo, Ti, and Nb were not detected.

Table 2. Chemical analysis of the samples before and after the distillation experiment.

Sample	Concentration (wt%)							
	Mg	Zn	Cr	Fe	Ni	Nb	Mo	Ti
Mg-Zn alloy	69.5	21.5	0.0006	0.02	8.92	0.0006	0.0005	0.0005
Distillation product	1.24	0.29	0.0088	0.12	98.3	0.0078	0.0034	0.0013
Alloy residue	0.29	0.02	38.5	40.99	2.86	10.31	5.67	1.36
Obtained Mg-Zn alloy	72.79	22.84	-	-	-	-	-	-

Note: Analyzed by ICP-OES.

The vacuum distillation experiment was carried out at 900 °C and 100 Pa for 6 h. Figures 13 and 14 give the XRD pattern and the SEM images of the alloy residue after distillation, respectively. As seen, the main phases in the alloy residue are Cr, Mo, and the intermetallic compound of Fe-Nb (Fe_2Nb) and Cr-Fe-Mo ($Cr_6Fe_{18}Mo_5$). The SEM image of the smooth surface of the alloy residue shows a rough surface with crevices and holes, and the fractured surface is porous and rough. As shown in Table 2, the concentration of Ni in the alloy residue is 2.86 wt% (the initial Ni concentration of the virgin superalloy is 52.6 wt%). The obtained product from distillation contained 98.3 wt% of Ni with 0.12 wt% Fe, which is relatively pure. In addition, the alloy residue after vacuum distillation became enriched in refractory metals, increasing the respective concentration of Nb from 4.8 wt% (virgin superalloy) to 10.31 wt%, Mo from 3.6 wt% (virgin superalloy) to 5.67 wt%, and Ti from 0.6 wt% (virgin superalloy) to 1.36 wt%. Furthermore, the alloy residue is brittle and can be easily crushed, which is beneficial for the subsequent separation processes. The

obtained Mg-Zn alloy from distillation contained 72.79 wt% of Mg and 22.84 wt% of Zn, and the recovery rate of Mg-Zn alloy was 94.8%.
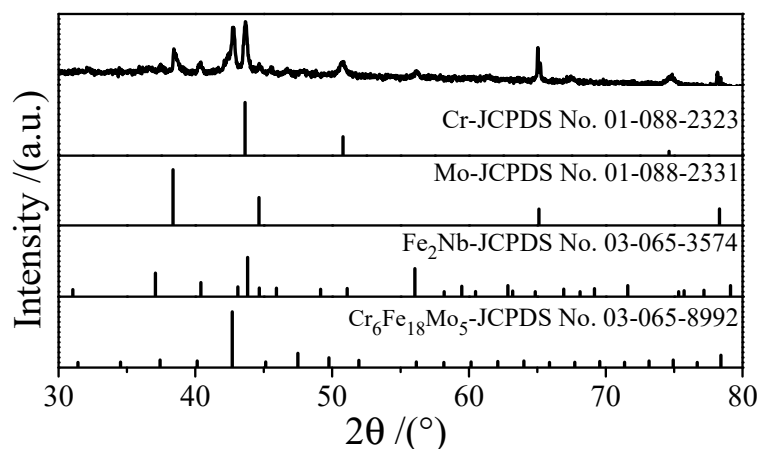

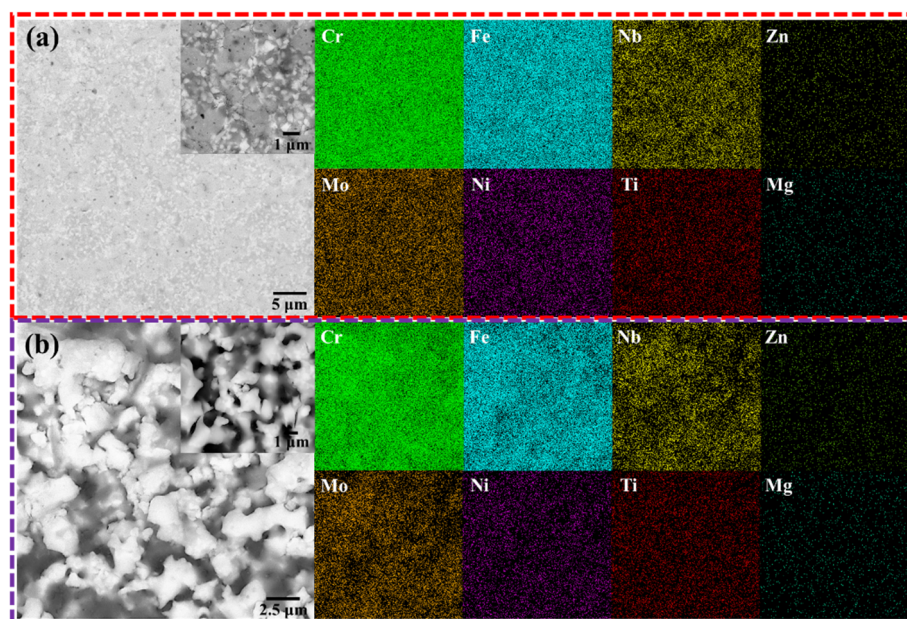**Figure 13.** XRD patterns of the alloy residue.

Figure 14. SEM images and EDS mapping of the alloy residue after vacuum distillation: (**a**) smooth surface; (**b**) fracture surface.

Compared to the traditional processes, the proposed method involving liquid metal extraction and vacuum distillation is highly effective towards selective extraction of Ni from the Ni-based superalloy. The process does not produce any waste gas or solid, which is environmentally friendly. In addition, the liquid metal extraction medium (i.e., Mg-Zn alloy) can be recycled and reused in the LME-VD process, thereby significantly reducing the material cost. The usage of the binary molten Mg-Zn offered the following advantages compared with the use of pure Mg as the extraction medium: (1) molten Mg can be easily oxidized at high temperature, and the addition of Zn forming Mg-Zn alloy can potentially reduce the degree of oxidation of Mg; (2) Mg-Zn alloy has a lower melting point, which helps further reduce the energy consumption by potentially lowering the operating temperature; (3) The operation condition of Mg-Zn alloy is relatively simpler due to the lower requirement on materials handling, and it should be easier for industrial application.

4. Conclusions

A new process with high efficiency and selectivity towards nickel extraction from superalloy scraps using molten Mg-Zn as an extractant was proposed and studied. The extraction rates of 97.1% for nickel and 0.62% for iron, with a very low extraction of chromium and the refractory metals (Nb, Mo, and Ti), were obtained under the following optimal conditions: heating temperature 800 °C, heating time 240 min, Mg/Zn molar ratio 9/1, and the Mg-Zn/superalloy mass ratio 5/1. Vacuum distillation was carried out on the upper part of the Mg-Zn-Ni alloy at 900 °C and 100 Pa for 6 h. A metal residue containing Ni of 98.3 mass pct was obtained. These results confirm that molten Mg-Zn can effectively extract Ni from the superalloys. The proposed process demonstrated its high efficiency and environmental friendliness for recycling Ni-based superalloys and other alloys. A general application of this approach can be explored for reclaiming valuable metals from other metallic secondary resources (such as electronic scraps, NdFeB magnet scraps, etc.) by identifying a suitable binary metal system.

Supplementary Materials: The following are available online at https://www.mdpi.com/article/10.3390/met11060993/s1, Figure S1: Zn-Ni binary phase diagram, Figure S2: Mg-Ni binary phase diagram, Figure S3: Mg-Zn binary phase diagram, Figure S4: Vapor pressures of selected metals as a function of reciprocal temperature, Figure S5: XRD patterns for Mg-Zn alloy of the samples under different heating temperature, Figure S6: XRD patterns for Mg-Zn alloy of the samples under different mass ratio of Mg-Zn to superalloy, Figure S7: XRD patterns for Mg-Zn alloy of the samples under different heating time.

Institutional Review Board Statement: Not applicable.

Informed Consent Statement: Not applicable.

Data Availability Statement: Data is contained within the article.

Conflicts of Interest: The authors declare no conflict of interest.

References

1. Makuza, B.; Tian, Q.H.; Guo, X.Y.; Chattopadhyay, K.; Yu, D.W. Pyrometallurgical options for recycling spent lithium-ion batteries: A comprehensive review. *J. Power Sources* **2021**, *491*, 229622. [CrossRef]
2. Zhu, H.J. Exploration laterite-nickel ore and analysis on utilization technology. *World Nonferrous Metals* **2007**, *10*, 7–10.
3. Pollock, T.M.; Tin, S. Nickel-based superalloys for advanced turbine engines: Chemistry, microstructure, and properties. *J. Propul. Power* **2006**, *22*, 361–374. [CrossRef]
4. Feng, R.S.; Xu, S.M. Research progress on recycling technology of indissoluble alloy with high melting point. *Hydrometall. China* **2012**, *31*, 338. (In Chinese)
5. Donachie, M.J.; Donachie, S.J. *Superalloys: A Technical Guide*, 2nd ed.; ASM International: Materials Park, OH, USA, 2002.
6. Greenfield, A.; Graedel, T.E. The omnivorous diet of modern technology. *Resour. Conserv. Recy.* **2013**, *74*, 1–7. [CrossRef]
7. Liu, Z.G.; Sun, T.C.; Wang, X.P.; Gao, E.X. Generation process of FeS and its inhibition mechanism on iron mineral reduction in selective direct reduction of laterite nickel ore. *Int. J. Min. Met. Mater.* **2015**, *22*, 901–906. [CrossRef]
8. Li, Y.J.; Yu, H.C.; Wang, D.Q.; Yin, W.X.; Bai, Y.S. The current status of laterite ore resources and its processing technology. *Met. Mine* **2010**, *11*, 5–9.
9. Oxley, A.; Barcza, N. Hydro-pyro integration in the processing of nickel laterites. *Miner. Eng.* **2013**, *54*, 2–13. [CrossRef]
10. Cui, F.H.; Mu, W.N.; Wang, S.; Xin, H.X.; Shen, H.T.; Xu, Q.; Zhai, Y.C.; Luo, S.H. Synchronous extractions of nickel, copper, and cobalt by selective chlorinating roasting and water leaching to low-grade nickel-copper matte. *Sep. Purif. Technol.* **2018**, *195*, 149–162. [CrossRef]
11. Woulds, M.J. Recycling of Engine Serviced Superalloys. *Superalloys* **1980**, 31–41. [CrossRef]

12. deBarbadillo, J.J. Nickel-base superalloys; physical metallurgy of recycling. *Metall. Trans. A* **1983**, *14*, 329–341. [CrossRef]

13. Schlatter, R. Melting and refining technology of high temperature steels and superalloys: A review of recent process developments. *Superalloys* **1972**, A1–A40. [CrossRef]

14. Fedika, A.A. Electro slag remelting. In Proceedings of the 2nd All Union Conference on Electro Slag Remelting, Metallurgiya, Moscow, Russia; 1969; p. 126.

15. Kim, M.S.; Lee, J.C.; Kim, E.Y.; Yoo, Y.S. Leaching of CMSX-4 superalloy in hydrochloric acid solutions. *J. Korean Inst. Resour. Recycl.* **2010**, *19*, 25–30.

16. Kim, M.S.; Lee, J.C.; Park, H.S.S.; Jun, M.J.; Kim, B.S. A multistep leaching of nickel-based superalloy scrap for selective dissolution of its constituent metals in hydrochloric acid solutions. *Hydrometallurgy* **2018**, *176*, 235–242. [CrossRef]

17. Fan, X.X.; Xing, W.D.; Dong, H.G.; Zhao, J.C.; Wu, Y.D.; Li, B.J.; Tong, W.F.; Wu, X.F. Factors research on the influence of leaching rate of nickel and cobalt from waste superalloys with sulfuric acid. *IJNM* **2013**, *2*, 63–67. [CrossRef]

18. Hall, J.D. Method of Preparation of metal Salts. U.S. Patent 2,716,588, 30 August 1955.

19. Ferron, C.G.; Seeley, L.E. Rhenium recovery. U.S. Patent 8,956,582, 24 March 2015.

20. Mamo, S.K.; Elie, M.; Baron, M.G.; Simons, A.M.; Gonzalez-Rodriguez, J. Leaching kinetics, separation, and recovery of rhenium and component metals from CMSX-4 superalloys using hydrometallurgical processes. *Separ. Purif. Technol.* **2019**, *212*, 150–160. [CrossRef]

21. Liu, Y.; Deng, L.; Liu, L.; Zhou, W.Z.; Chang, Y.L. Adsorption of Re from Electrolyte of Superalloy by Using D296 Resin. *Rare Metals* **2017**, *41*, 679. (In Chinese)

22. Armin, O. Recycling of Superalloys with the Aid of an Alkali Metal Salt Bath. U.S. Patent 0255372 A1, 15 October 2009.

23. Heshmatpour, B.; Mcdonald, R. Recovery and refining of rhenium, tungsten and molybdenum from W-Re, Mo-Re and other alloy scraps. *J. Less Common. Met.* **1982**, *86*, 121–128. [CrossRef]

24. Atkinson, G.B.; Nicks, L.J. Leaching aluminum superalloy melts with hydrochloric and sulfuric acids. *Resour. Conserv. Recy.* **1986**, *9*, 197–209. [CrossRef]

25. Hilliard, H.E. Recycling Superalloy Scrap by Vapor Phase Zinc Embrittlement. U.S. Patent 4718939-A, 12 January 1988.

26. Iskander, A.A.; Bjorling, G.E.; Agden, J.S. Process for Recovery from Secondary Material of Such Metals as Nickel Cobalt Iron and Copper Said secondary MATERIAL Comprising in Addition One or More Metals Having a high MELTING Point. U.S. Patent 3649487, 14 March 1972.

27. Guo, X.Y.; Zhang, C.X.; Tian, Q.H.; Yu, D.W. Liquid Metals Dealloying as a General Approach for the Selective Extraction of Metals and the Fabrication of Nanoporous Metals: A review. *Mater. Today Commun.* **2021**, *26*, 102007. [CrossRef]

28. Yagi, R.; Okabe, T.H. Recovery of Nickel from Nickel-Based Superalloy Scraps by Utilizing Molten Zinc. *Metall. Mater. Trans. B* **2017**, *48*, 335–345. [CrossRef]

29. Cui, F.H.; Wang, G.; Yu, D.W.; Gan, X.D.; Tian, Q.H.; Guo, X.Y. Towards "zero waste" extraction of nickel from scrap nickel-based superalloy using magnesium. *J. Clean. Prod.* **2020**, *262*, 121275. [CrossRef]

30. Lee, D.W.; Lee, H.; Shin, S.; Wang, J.P. Nickel Recycling by Magnesium Reaction of Fe-Ni Alloy Scrap. *Adv. Mater. Res.* **2014**, *1025*, 519–524. [CrossRef]

31. Lee, D.W.; Yu, J.H.; Jang, T.S.; Kim, B.K. Nanocrystalline iron particles synthesized by chemical vapor condensation without chilling. *Mater. Lett.* **2005**, *59*, 2124–2127. [CrossRef]

32. Bale, C.W.; Chartrand, P.; Degterov, S.A.; Eriksson, G.; Hack, K.; Mahfoud, R.B.; Melançon, J.; Pelton, A.D.; Petersen, S. Factsage thermochenical software and databases. *Calphad* **2016**, *54*, 35–53. [CrossRef]

33. Nayeb-Hashemi, A.A.; Clark, J.B.; Swartzendruber, L.J. The Fe-Mg (Iron-Magnesium) system. *Bull. Alloy Phase Diagr.* **1985**, *6*, 335–336. [CrossRef]

34. Su, X.P.; Tang, N.Y.; Toguri, J.M. Thermodynamic evaluation of the Fe-Zn system. *J. Alloys Compd.* **2001**, *325*, 129–136. [CrossRef]

35. Yu, D.W.; Gan, X.D.; Cui, F.H.; Guo, X.Y.; Tian, Q.H. Dissolution behavior of nickel-based superalloy in molten zinc: Its mechanism and kinetics. *J. Alloys Compd.* **2021**, *878*, 160338. [CrossRef]

36. Bhan, S.; Jain, K.C.; Lal, A. The Mg-Ni-Zn System (Magnesium-Nickel-Zinc). *J. Phase Equilib.* **1997**, *18*, 305. [CrossRef]

37. Wang, P.S.; Zhao, J.R.; Du, Y.; Xu, H.H.; Gang, T.; Fen, J.C.; Zhang, L.J.; He, C.Y.; Liu, S.H.; Ouyang, H.W. Experimental investigation and thermodynamic calculation of the Fe-Mg-Mn and Fe-Mg-Ni systems. *Int. J. Mater. Res.* **2011**, *102*, 6–16. [CrossRef]

38. Xu, K.; Liu, S.H.; Du, Y.; Dreval, L.Y.; Cai, G.M.; Jin, Z.P. Thermodynamic investigation of the Mg-Ni-Zn system by experiments and calculations and its application. *J. Alloys Compd.* **2019**, *784*, 769–787. [CrossRef]

39. Niu, H.Y.; Deng, K.K.; Nie, K.B.; Cao, F.F.; Zhang, X.C.; Li, W.G. Microstructure, mechanical properties and corrosion properties of Mg-4Zn-xNi alloys for degradable fracturing ball applications. *J. Alloys Compd.* **2019**, *787*, 1290–1300. [CrossRef]